Title: Climate explains geographic and temporal variation in mosquito-borne disease dynamics on two continents

Jamie M. Caldwell[1], A. Desiree LaBeaud[2], Eric F. Lambin[3,4], Anna M. Stewart-Ibarra[5,6], Bryson A. Ndenga[7], Francis M. Mutuku[8], Amy R. Krystosik[2], Efraín Beltrán Ayala[9], Assaf Anyamba[10], Mercy J. Borbor-Cordova[11], Richard Damoah[12], Elysse N. Grossi-Soyster[2], Froilán Heras Heras[13], Harun N. Ngugi[14,15], Sadie J. Ryan[16-18], Melisa M. Shah[19], Rachel Sippy[13,20,21], Erin A. Mordecai[1]

[1] Department of Biology, Stanford University, 371 Serra Mall, Stanford, California, USA

[2] Department of Pediatrics, Division of Infectious Diseases, Stanford University, 300 Pasteur Drive, Stanford, California, USA

[3] School of Earth, Energy & Environmental Sciences, and Woods Institute for the Environment, Stanford University, Stanford, California 94305, USA.

[4] Georges Lemaître Earth and Climate Research Centre, Earth and Life Institute, Université catholique de Louvain, 1348 Louvain-la-Neuve, Belgium.

[5] Department of Medicine and Department of Public Health and Preventative Medicine, SUNY Upstate Medical University, Syracuse, NY, USA

[6] InterAmerican Institute for Global Change Research (IAI), Montevideo, Uruguay

[7] Centre for Global Health Research, Kenya Medical Research Institute, Kisumu, Kenya

[8] Department of environment and health sciences, technical university of Mombasa, Mombasa, Kenya

[9] Technical University of Machala, Machala, Ecuador

[10] Universities Space Research Association and NASA Goddard Space Flight Center, Greenbelt, MD, USA.

[11] Facultad de Ingeniería Marítima y Ciencias del Mar, Escuela Superior Politécnica del Litoral, ESPOL, Guayaquil, Ecuador

[12] Morgan State University and NASA Goddard Space Flight Center, Greenbelt, MD, USA.

[13] Center for Research SUNY-Upstate-Teófilo Dávila Hospital, Machala, Ecuador

[14] Department of Biological Sciences, Chuka University, Chuka, Kenya

[15] Department of Zoology, School of Biological Sciences University of Nairobi, Nairobi, Kenya

[16] Emerging Pathogens Institute, University of Florida, Gainesville, Florida

[17] Quantitative Disease Ecology and Conservation (QDEC) Lab, Department of Geography, University of Florida, Gainesville, Florida;

[18] School of Life Sciences, University of KwaZulu, Natal, South Africa

[19] Department of Medicine, Division of Infectious Diseases, Stanford University, 300 Pasteur Drive, Stanford, California, USA

[20] Institute for Global Health and Translational Science, SUNY-Upstate Medical University, Syracuse, NY, USA

[21] Department of Medical Geography, University of Florida, Gainesville, FL, USA

Abstract:

Climate drives population dynamics, but when the underlying mechanisms are unresolved, studies can lead to seemingly context-dependent effects of climate on natural populations. For climate-sensitive vector-borne diseases such as dengue, chikungunya, and Zika, climate appears to have opposing effects in different contexts. In this study, our objective was to test the extent to which a mathematical model, parameterized with climate-driven mosquito physiology measured in laboratory studies, predicts observed vector and disease dynamics in the field across ecologically and culturally distinct settings in Ecuador and Kenya. The model incorporates different rainfall functions and time lags. We show that the climate-driven model captures three key epidemic characteristics across settings: the number, timing, and duration of outbreaks. In addition, the model generates a range of disease dynamics consistent with observations of *Aedes aegypti* abundances and laboratory-confirmed arboviral incidence with varying levels of accuracy (28 – 85% for vector dynamics, 44 – 88% for human disease dynamics). Further, we find that the model predicted vector dynamics better in sites with a smaller proportion of young children in the population, lower mean temperature, and a larger proportion of homes with piped water and made of cement. A mechanistic model with limited calibration to local data that robustly captures the influence of climate on viruses transmitted by *Aedes aegypti* provides critical information to help guide future intervention efforts and improve disease projections associated with climate change.

Introduction:

Climate is a major driver of species interactions and population dynamics, but the mechanisms underlying the ecological effects of climate are often poorly understood and rarely tested in the field [1]. One of the primary ways that climate impacts populations is through its effects on species' vital rates [2]. However, the effects of climate on population dynamics may appear context dependent in the field because multiple climate variables can act synergistically, with each climate variable potentially affecting multiple vital rates, and their impacts may be nonlinear, changing direction and relative importance across a gradient of conditions [3,4]. Therefore, paradoxically, while climate is thought to be one of the most pervasive drivers of ecological processes, its directional and dynamical effects on systems are often poorly understood and difficult to predict. Vector-borne diseases provide an interesting case study to test whether climate sensitive traits measured in controlled, laboratory settings can reproduce the wide range of dynamics observed in the field. For example, transmission of mosquito-borne viral (arboviral) diseases such as dengue, chikungunya, and Zika occur along a spectrum from low levels of year-round endemic transmission [5] to large seasonal or interannual outbreaks [6]. We hypothesize that important features of these differing dynamics arise due to regional or seasonal differences in climate, where the magnitude and direction of the effects of climate on vector and disease dynamics differ [7–12].

Understanding the mechanisms that drive disease dynamics can help address two critically important research priorities for arboviruses like dengue, chikungunya, and Zika: assessing intervention strategies and projecting climate change impacts on disease

93 dynamics. While phenomenological models often replicate arboviral disease dynamics
94 remarkably well [13], mechanistic models that do not rely on local data for calibration
95 and capture mosquito population dynamics and interactions between mosquitoes and
96 humans will provide more realistic projections for epidemic dynamics across a broad
97 range of transmission settings. With no widely available vaccine, vector control (e.g.,
98 larvicides, *Wolbachia*-infected mosquito releases) remains the primary method for
99 preventing arboviral disease transmission, and, like other vector-borne diseases with
100 complex transmission dynamics, model simulations can help guide effective intervention
101 efforts [14,15]. Further, mechanistic models are better suited to predict how climate
102 change will impact future disease burden and distribution, as projected climate conditions
103 are outside the current arboviral climate niche space [16]. Despite the potential usefulness
104 of mechanistic approaches, validation with vector and disease data are limited, raising an
105 important question about which epidemic characteristics, if any, we should expect a
106 model to capture when the model was parameterized with data that is on different scales
107 (e.g., individuals versus populations) and independent from the transmission system we
108 wish to predict. Thus, because we cannot study epidemic dynamics in every possible
109 transmission setting, it becomes important to understand the extent to which models
110 derived from fundamental and laboratory-measured traits explain disease dynamics
111 across diverse settings.
112
113 We hypothesize that a climate-driven mechanistic model with limited calibration should
114 capture many important characteristics of disease dynamics for dengue, chikungunya, and
115 Zika because of the ecology of *Aedes aegypti*, the primary disease vector. *Ae. aegypti* are

116 anthropophilic, globally distributed mosquitoes that breed in artificial containers with
117 standing water [17,18]. All mosquito and parasite traits that are important for
118 transmission and linked to metabolism, such as reproduction, development, survival,
119 biting rate, and extrinsic incubation period, are temperature dependent with an
120 intermediate thermal optimum [19–21]. Humidity is positively associated with mosquito
121 survival because the high surface area to volume ratio of mosquitoes exposes them to
122 desiccation [22,23]. Standing water from rainfall provides essential larval and pupal
123 habitat for mosquitoes, but the relationship is complex because heavy rainfall can flush
124 away breeding habitats [24–26] and water storage practices during drought can increase
125 water availability, mosquito abundance, and contact between mosquitoes and people [27–
126 29]. A previous simulation study predicted that in settings with suitable climate for
127 transmission throughout the year (e.g., mean temperature = 25°C; range = 20 – 30°C),
128 temperature drives the timing and duration of outbreaks, but not the maximum number of
129 infections or final epidemic size [30]. This finding suggests that a model that incorporates
130 temperature-dependent vector traits should capture some important epidemic
131 characteristics.
132
133 In this study, our goal was to test the extent to which climate-driven mosquito traits drive
134 disease dynamics across two geographically distinct regions and to characterize
135 additional climatological, ecological, and social factors that may mediate the effects of
136 climate on disease dynamics. We built on previous mechanistic and semi-mechanistic
137 models that incorporate the *Aedes* mosquito life cycle and human disease dynamics [30–
138 35] by combining a suite of temperature, humidity, and rainfall dependent trait functions

into one epidemiological model. We validated the model with *Ae. aegypti* abundances and laboratory-confirmed dengue, chikungunya, and Zika cases from two equatorial countries with distinct socioeconomic, geographic, cultural, and disease transmission settings: Ecuador and Kenya (Fig. 1, Table 1). The study sites within each country were distributed across a gradient of temperature, humidity, and rainfall. Previous studies have found that *Ae. aegypti* and dengue were positively associated with warm and wet conditions in Ecuador and Kenya [6,36–38], although other *Ae. aegpyti*-vectored arboviruses in Kenya such as chikungunya have been associated with warm and dry conditions [39]. Both countries have all four dengue serotypes circulating and have recently experienced outbreaks of chikungunya; yet, arboviral transmission dynamics differ in each country. In Ecuador, dengue is a re-emerging disease with large seasonal epidemics that frequently result in severe dengue [6]; by contrast, in Kenya, dengue is transmitted at low levels year-round [5] and intermittent self-limiting outbreaks often go undetected [40]. Further, compared with South America, severe dengue is rare in sub-Saharan Africa, perhaps because African strains of *Ae. aegpyti* have lower susceptibility to all four dengue serotypes [41], and/or because people of African ancestry are less susceptible to severe dengue [42].

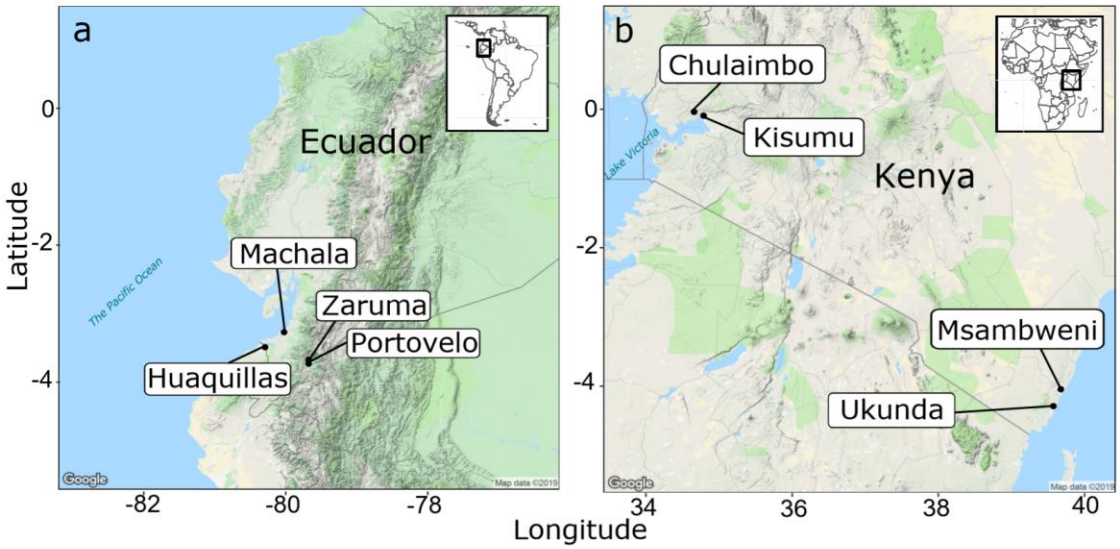

Figure 1: Study sites within two equatorial countries: (a) Ecuador in South America and (b) Kenya in East Africa.

Table 1: Study sites differ geographically, climatologically, and socioeconomically. [1]Mean annual normalized difference vegetation index (NDVI) is a proxy for photosynthesis and measured as a difference in spectral reflectance in the visible and near-infrared regions from NASA/NOAA MODIS (MOD13A1) [43]. [2]Dominant land cover type is measured and classified from spectral and temporal features from NASA/NOAA MODIS (MCD12Q1) [44]. Land cover types include (9) Tree cover 10 - 30%, (10) Dominated by herbaceous annuals, (13) >30% impervious surface area, and (14) 40 - 60% mosaics of small-scale cultivation. Bed net use represents availability of and/or willingness to adopt intervention strategies for preventing infection rather than a direct adaptive response to preventing infection by day-biting *Ae. aegpyti* mosquitoes.

	Huaquillas, Ecuador	Machala, Ecuador	Portovelo, Ecuador	Zaruma, Ecuador	Chulaimbo, Kenya	Kisumu, Kenya	Msmabweni, Kenya	Ukunda, Kenya
Site characteristics								
Elevation (m)	15	6	645	1,155	1,328	1,100	4	8
Location	Coastal	Coastal	Inland	Inland	Inland	Inland	Coastal	Coastal
Mean annual NDVI[1]	0.22	0.12	0.61	0.57	0.63	0.35	0.33	0.52
Dominant land cover type[2]	13	13	9	10	14	13	13	10
Climate								
Mean temperature (°C)	26	26	25	22	24	26	28	28
Mean relative humidity (%)	81	84	81	86	69	50	76	78
Mean annual rainfall (mm)	317	669	500	1115	1125	810	1048	922
Demographics								
Human population size	57,366	279,887	13,673	25,615	7,304	491,893	15,371	80,193
Population <5 years (%)	10	9	9	8	12	12	13	14
Population of African ancestry (%)	5.1	6.0	3.3	2.9	100.0	100.0	100.0	100.0
Housing quality (% houses)								
Piped water inside home	90	91	100	96	2	4	3	11
No screens on windows	7	60	91	99	74	78	43	21
House materials (cement/mud/wood)	87/5/0	87/8/5	95/0/5	93/1/1	29/70/0	77/17/0	38/62/0	51/47/0
Exposure, vulnerability, and adaptive capacity								
Arboviruses present	dengue, chikungunya, Zika				>200 documented including dengue, chikungunya, Yellow fever, Rift Valley fever, West Nile fever, O'nyong-nyong			
Insecticide use (% houses)	19	28	46	37	0	0	11	55
Bednet use (% houses)	77	55	15	21	93	92	0	96
Other vector control strategies used	Ultra-low volume fumigation with malathion (organophosphate) and community mobilization to eliminate larval habitats				Mosquito coils			
Annual gross domestic product by country (2018)	$177 billion USD				$85.98 billion USD			

Results:

Capturing key epidemic characteristics

The dynamic susceptible, exposed, infectious – susceptible, exposed, infectious, removed (SEI-SEIR) compartmental model parameterized with temperature-, humidity-, and rainfall-dependent mosquito life history traits (Fig. 2) reproduced three key characteristics of epidemics: number of outbreaks, timing of outbreak peak, and duration

of outbreaks. We defined an outbreak as a continuous time period with peak cases exceeding the mean number of cases (predicted or observed) plus one standard deviation within a site. Across all sites, the number of outbreaks predicted by the model closely matched the number of outbreaks observed ($R^2 = 0.79$, $p < 0.01$; Fig. 3a). Supporting our *a priori* expectations based on a previous simulation study [30], we found that the climate-driven model predicted peak timing of outbreaks ($R^2 = 0.71$, $p < 0.01$; Fig. 3b) and outbreak duration ($R^2 = 0.51$, $p < 0.01$; Fig. 3c) well but did not predict the final outbreak size (Fig. 3d) or maximum number of infections (Fig. 3e) across sites. Overall, the model predicted four outbreaks that were not observed and did not predict five outbreaks that occurred. The model may miss an outbreak (i.e., false negatives) when, for example, suitable climate occurs but the pathogen is not introduced or the susceptible population is depleted from previous outbreaks.

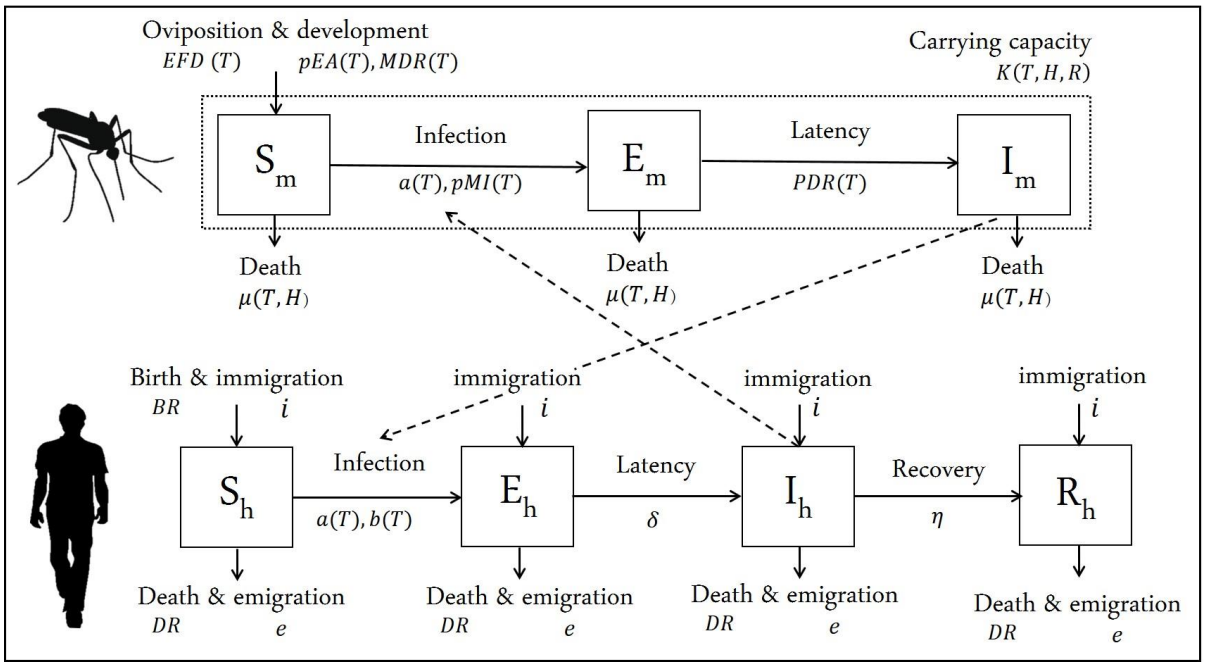

193 **Figure 2: SEI-SEIR epidemiological model framework.** The mosquito population is
194 split among susceptible (S_m), exposed (E_m), and infectious (I_m) compartments (squares)
195 and the human population is split among susceptible (S_h), exposed (E_h), infectious (I_h),
196 and recovered (R_h) compartments. Solid arrows indicate the direction individuals can
197 move between classes and dashed arrows indicate the direction of transmission.
198 Transitions among compartments are labeled by the appropriate processes and
199 corresponding rate parameters (see Methods for parameter definitions and more detail).
200 Rate parameters with a T, H, and R are temperature-, humidity-, and rainfall-dependent,
201 respectively. The total adult mosquito population (S_m, E_m, and I_m compartments; dotted
202 rectangle) is maintained at an abundance less than or equal to the mosquito carrying
203 capacity.
204
205

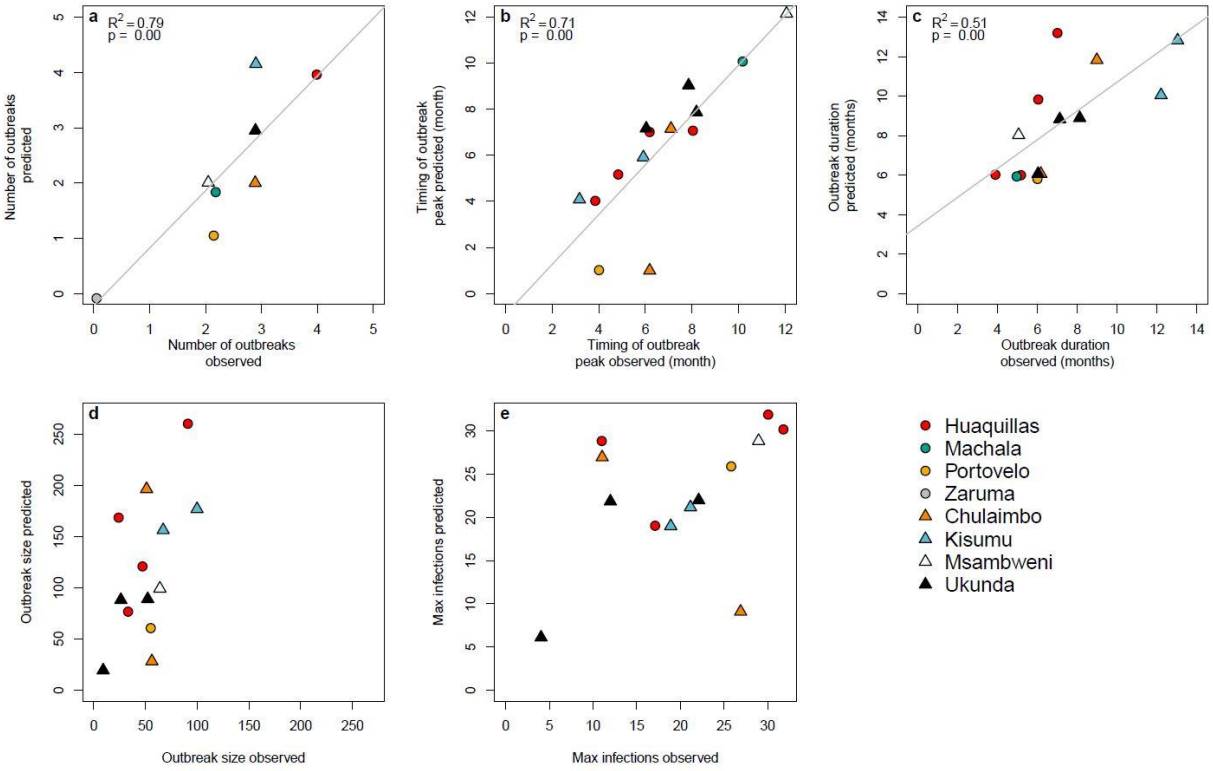

Figure 3: Model predictions for the number, timing, and duration of arboviral outbreaks closely matched field observations. Scatterplots show model predictions versus observations for different epidemic characteristics. (a) Number of outbreaks indicates the total number of predicted and observed outbreaks in a site over the study period. (b) Timing of outbreak peak, (c) outbreak duration, (d) outbreak size, and (e) maximum infections (e.g., max I_h during an outbreak) correspond to individual outbreaks where model predictions and observations overlapped in time, therefore, some plots show multiple data points per site. Outbreaks are colored by site with different symbols for Ecuador (circles) and Kenya (triangles). We show regression lines and associated statistics for statistically significant relationships. For visualization purposes, we jittered the data points to show overlapping data and we excluded data from Machala in plots (d)

outbreak size and (e) maximum infections because the magnitude differed substantially from all other sites.

Capturing spatio-temporal disease dynamics across sites

The SEI-SEIR model generated mosquito and disease dynamics that better reflected observed dynamics in some sites than others (Fig. 4, Table 2). Model-predicted mosquito abundances were significantly correlated with field-collected observations of mosquito abundances in all eight study sites, explaining 28 – 85% of site-level variation through time based on pairwise correlations with an adjusted p-value for time series data (following [45]). Based on surveys conducted across all vector life stages in Kenya (only adult mosquitoes were collected in the Ecuador surveys), the SEI-SEIR model explained variation in the abundance of adult mosquitoes (28 – 63%) better than pupae (25 – 32%), late instars (30 – 33%), early instars (20 – 36%), and eggs (33 – 55%), likely because the model did not explicitly incorporate other mosquito life history stages. Model-predicted disease cases were significantly correlated with laboratory-confirmed arboviral incidence in seven of the eight study sites, explaining 44 – 88% of site-level variation through time (within sites with statistically significant pairwise correlations). We confirmed that the predicted dynamics were stable with sensitivity analyses to initial conditions (see Methods), as emerging diseases can display chaotic dynamics due to a high sensitivity to initial conditions. Overall, the model reproduced disease dynamics slightly better for sites in Ecuador compared with Kenya.

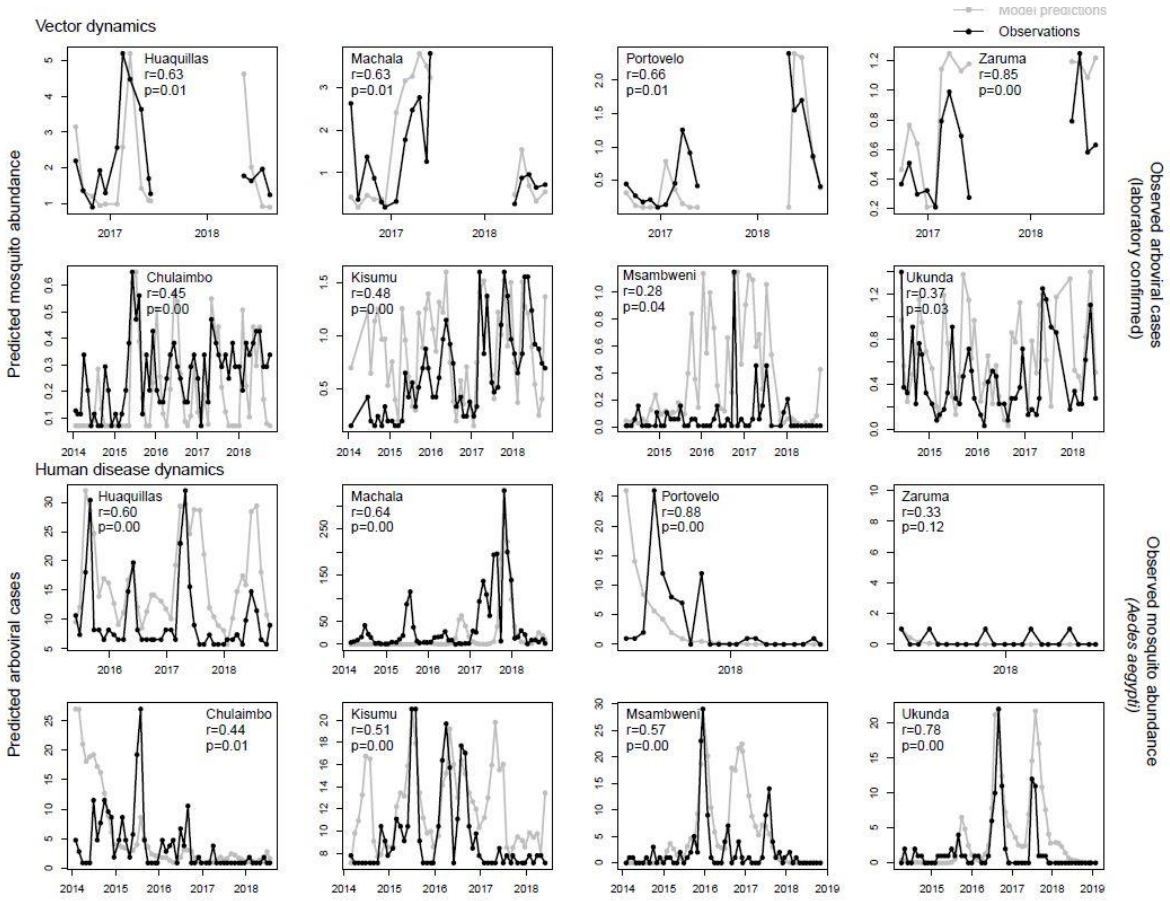

241

242 **Figure 4: Model predicts vector and human disease dynamics better in some settings**
243 **than others.** Each plot shows the time series of SEI-SEIR model predictions (grey dots
244 connected by grey lines) and field observations (black dots connected by black lines) for
245 vector (top two rows) and human disease (bottom two rows) dynamics for each study site
246 with the pairwise correlation (r) and adjusted p-value (p). We calculated observed
247 mosquito abundances as the mean number of adult *Ae. aegypti* per house, month, year,
248 and site. We calculated observed arboviral cases as the total number of laboratory-
249 confirmed dengue (any serotype), chikungunya, and Zika cases per month, year, and site;
250 six of the eight study sites only included dengue cases (see Methods). The first and third
251 rows show sites in Ecuador and the second and fourth rows show sites in Kenya. We
252 show uncertainty in model predictions in Figs. S1-2.

Table 2: Model predictions reflect a range of observed transmission dynamics when incorporating different rainfall functions and time lags across sites. For each study site, we calculated pairwise correlations between time series of field observations (*Ae. aegypti* abundances or arboviral cases) and time series of model predictions for the SEI-SEIR model with one of three rain functions for mosquito carrying capacity (Brière, Inverse, or Quadratic) and six time lags (0-5 months). This table shows specifications for the model (e.g., rain function and time lag) with the highest pairwise correlation value, r, for each study site and observation type (vectors or human disease cases), as well as the statistical significance of the correlation value (adjusted p-value) based on the Modified Chelton method [45] to account for temporal autocorrelation.

	Vector dynamics				Human disease dynamics			
Site	Rainfall function	r	Adjusted p-value	Lag (months)	Rainfall function	r	Adjusted p-value	Lag (months)
Huaquillas, Ecuador	Quadratic	0.63	0.01	1	Inverse	0.60	0.00	2
Machala, Ecuador	Quadratic	0.63	0.01	0	Brière	0.64	0.00	4
Portovelo, Ecuador	Brière	0.66	0.01	1	Brière	0.88	0.00	3
Zaruma, Ecuador	Inverse	0.85	0.00	1	Inverse	0.33	0.12	0
Chulaimbo, Kenya	Inverse	0.45	0.00	1	Quadratic	0.36	0.02	4
Kisumu, Kenya	Brière	0.48	0.00	0	Quadratic	0.51	0.00	4
Msambweni, Kenya	Inverse	0.28	0.04	0	Inverse	0.57	0.00	3
Ukunda, Kenya	Inverse	0.37	0.03	1	Inverse	0.78	0.00	5

We found evidence that rainfall affects transmission through multiple mechanisms and at different time lags (Table 2). Since the effect of rainfall on mosquito abundances is not well understood, we simulated disease dynamics for each site three times, using one of

three hypothesized rainfall relationships (Brière, inverse, and quadratic; Fig. S3). We determined the best rainfall function and time lag for each site based on the highest pairwise correlation value between model predictions and observations. The model with the exponentially decreasing inverse rain function (Fig. S3c), which indicates that mosquito abundances peak when there is no or low rainfall (likely as a result of water storage practices and/or unreliable water sources) described observed mosquito and disease dynamics most often, especially in the Kenya sites (Table 2), where household access to piped water is very low (Table 1). The left-skewed unimodal Brière rainfall function (Fig. S3a), which indicates that mosquito abundances increase with increasing rainfall until some threshold where flushing occurs, described disease dynamics in some settings, particularly in the Ecuador sites. The symmetric unimodal quadratic rainfall function (Fig. S3b), which indicates that mosquito abundances peak with intermediate amounts of rainfall and are reduced with low and high rainfall values, also described disease dynamics in some settings. Interestingly, we did not find a single rainfall function that consistently described dynamics for mosquitoes or arboviral cases across study sites, or for both mosquitoes and arboviral cases within individual study sites (Table 2). In contrast, we did find some consistency with time lags. The model best predicted mosquito abundances in the same month or one month in the future. In more than half of the sites, the model best predicted human disease cases three to four months in the future, and in almost all sites at least two months in the future (the exception is Zaruma, where very few arbovirus cases were reported during the study period and were likely due to importation rather than local transmission). Given that multiple rainfall functions and time lags are supported by field data (even within the same study site), we propose a

290 conceptual model that incorporates multiple pathways for rainfall to affect disease
291 dynamics along a continuum of rainfall (Fig. 5), in contrast to distinct functional
292 relationships for a given setting, which motivated the approach used in this study.
293

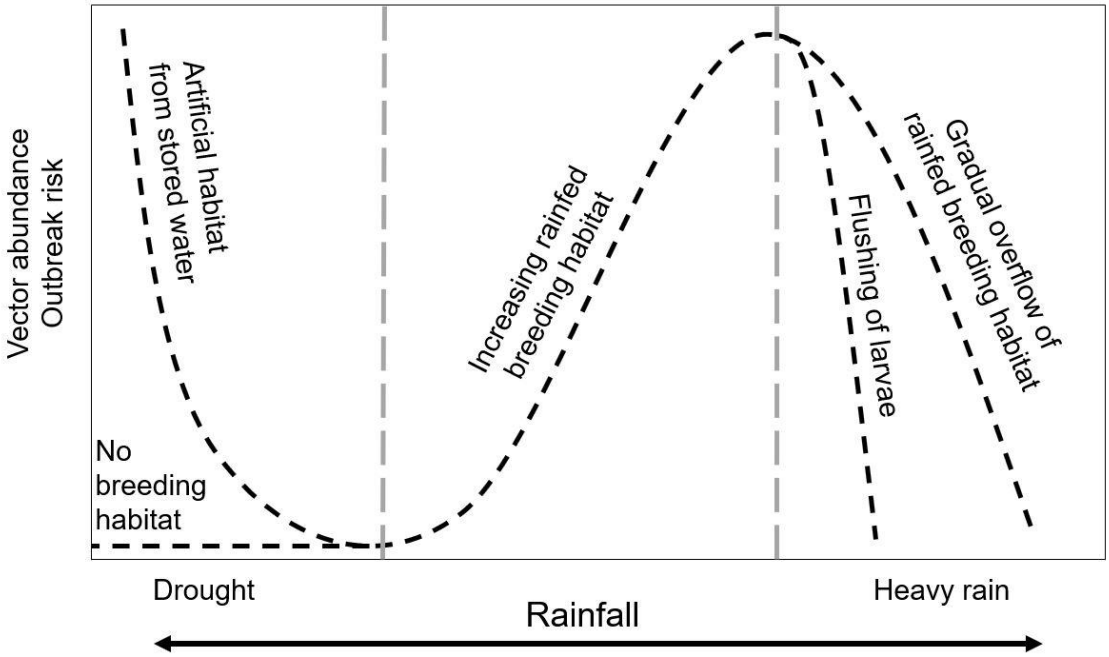

294

295 **Figure 5: Conceptual model for nonlinear functional relationships between rainfall**
296 **and vector abundance and arboviral outbreak risk.** Dashed lines show multiple
297 potential pathways for rainfall to affect transmission dynamics and include the functional
298 relationships supported in this study. Labels indicate the hypothesized mechanisms along
299 a gradient of rainfall. Adapted from [46].
300

301 ***Factors that mediate disease dynamics predictability***

302 The ability of the model to generate similar dynamics to those found in the field varied
303 with demography, housing quality, and climate. Although the sample size is small (N = 8

304 sites), we found that the SEI-SEIR model generally predicted vector dynamics better in
305 sites with a smaller proportion of young children in the population ($R^2 = 0.89$, $p < 0.01$;
306 Fig. 6a), lower mean temperature ($R^2 = 0.63$, $p < 0.05$; Fig. 6c), and a larger proportion of
307 homes with piped water ($R^2 = 0.76$, $p < 0.01$; Fig. 6b) and made of cement ($R^2 = 0.69$, p
308 < 0.05; Fig. 6d; list of all factors we assessed are provided in Table 1). Based on the
309 range of mean temperatures at our study sites (22 – 28°C), our findings indicate that
310 vector dynamics become less predictable as temperatures near the optimal temperature
311 for transmission (derived in previous studies as 29°C) following the shape and slope in
312 the R_0 curve (Fig. 7). This complements phenomenological models that have found
313 minimal effects of temperature near the empirically derived thermal optima (Fig. 7).
314 None of the socio-economic factors that we examined in this study (Table 1) explained
315 variability in the pairwise correlations for human disease cases among sites.
316

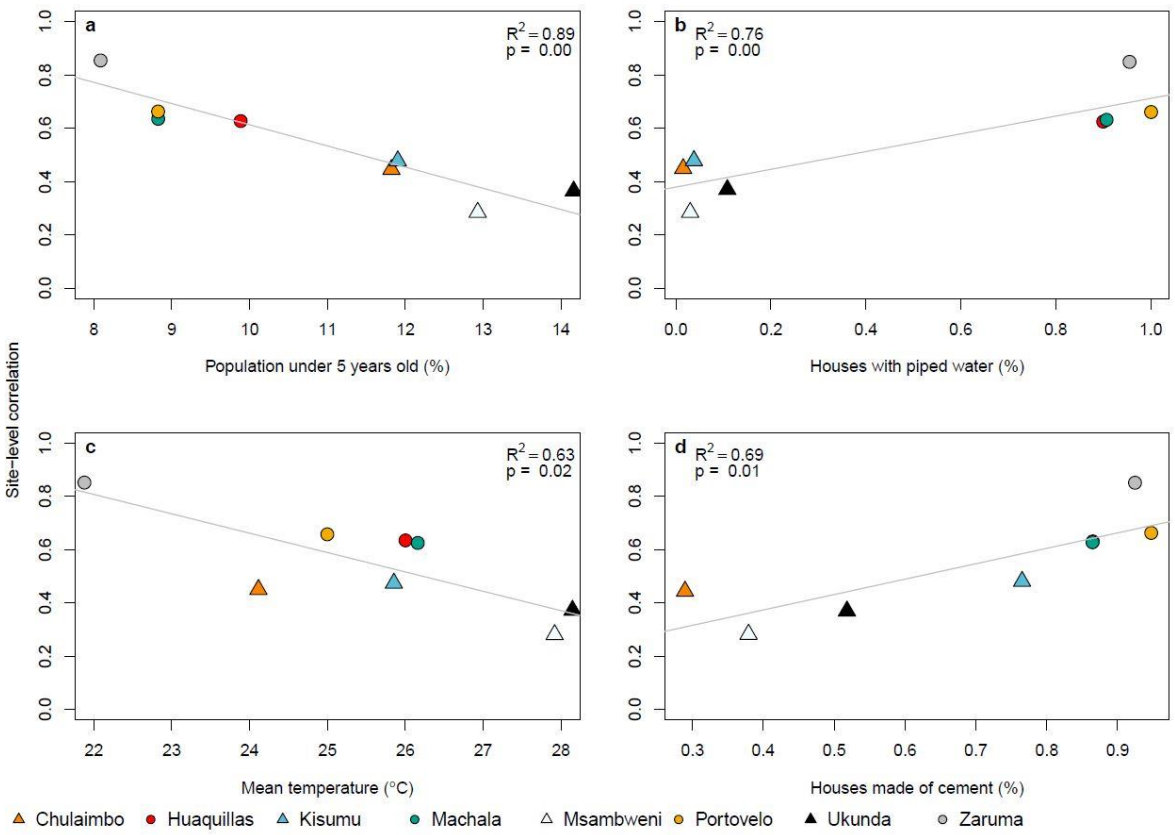

Figure 6: Demography, housing construction, and climate affect model predictive capacity for vectors. Factors that influence the predictability of vector dynamics include (a) proportion of the population under five years of age, (b) proportion of houses with piped water, (c) mean temperature, and (d) proportion of houses made with cement (walls and/or floors). Points indicate the pairwise correlation value for a single site (colors) with different symbols for Ecuador (circles) and Kenya (triangles). Each plot also shows the linear regression lines and associated statistics.

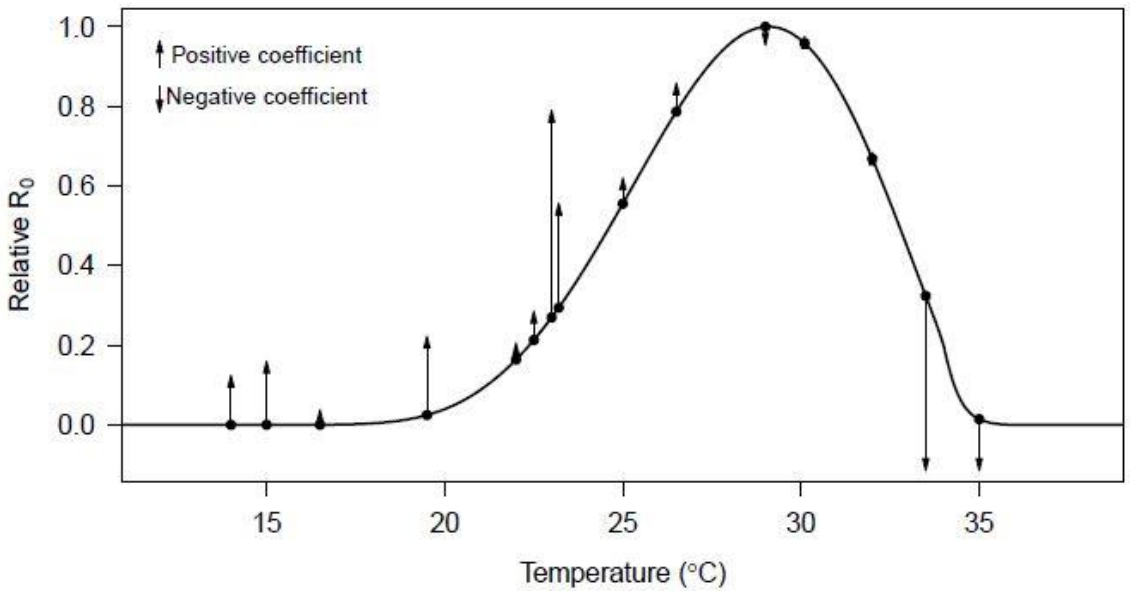

Figure 7: Independently predicted relative R_0 from a model derived from laboratory studies explains differences in the magnitude and direction of the effects of temperature on dengue transmission in the field across varied settings from previous studies. The black line shows the relative basic reproductive number (R_0, normalized to a 0-1 scale) plotted against temperature based on all temperature-dependent traits from [19] used in the SEI-SEIR model presented here. Points indicate mean temperature values from previous field-based statistical analyses that related dengue cases with minimum, maximum, or mean ambient temperature; arrows correspond to the direction (up = positive, down = negative) and relative effect size of the temperature – dengue relationship based on coefficient values from the following studies: [47,48,57,58,49–56]. See Methods and Table S1 for more detail. As expected, the largest observed positive effects of temperature occurred in the rapidly increasing portion of the R_0 curve (~22-25°C; consistent with findings in this study) and the largest observed negative effects occurred well above the predicted optimum, near the upper thermal limit (~33-35°C).

342

343 **Discussion:**

344 Directly observing the influence of climate on species interactions and population
345 dynamics is often challenging because of interacting and nonlinear relationships. Here,
346 we directly and quantitatively connect laboratory-based climate relationships to observed
347 mosquito and disease dynamics in the field, supporting the mechanistic role of climate in
348 these disease systems. The trait-based modeling approach captured several key epidemic
349 characteristics and generated a range of disease dynamics along a spectrum of settings
350 with low levels of transmission to seasonal outbreaks, helping to reconcile seemingly
351 context dependent effects (i.e., opposite conclusions about the magnitude and direction of
352 effects; Fig. 7) of climate on arboviral transmission dynamics from the literature [7–
353 12,47].

354

355 The results of this study shed some light on the influence of climate in driving endemic
356 versus epidemic dengue transmission. Although Ecuador typically experiences seasonal
357 epidemics [6] and Kenya typically experiences low levels of year-round transmission [5],
358 the sites within this study suggest that epidemic transmission is more common in settings
359 with clear seasonality (e.g., coastal sites) whereas endemic transmission is more common
360 in settings with more climate variability (e.g., inland sites), regardless of country. Coastal
361 sites experienced more regular seasonal climate cycles, likely because oceans buffer
362 climate variability, and this seasonality corresponded with seasonal epidemics. In
363 contrast, the inland sites experienced more day-to-day climate variability, which resulted
364 in more fluctuations in disease cases. As a result, the occurrence and persistence of

suitable temperature, rainfall, and humidity conditions enabling outbreaks were less regular in sites with more climate variability. The ability of the model to detect key epidemic characteristics across endemic and epidemic settings indicates that climate plays a major role in driving when outbreaks occur and how long they last.

Using field data on mosquitoes and disease cases from diverse settings and a model parameterized with data from other studies, we identified several key epidemic characteristics that we should (and should not) expect to capture in new settings. While we would never expect a perfect correlation between model predictions and observations, even if the model perfectly captured climate-host-vector dynamics because of the many additional factors that affect transmission in nature, our results indicate that a model with limited calibration can determine the number of outbreaks across settings remarkably well (Fig. 3a). This finding could be particularly useful for prioritizing surveillance or intervention activities across a range of a potential sites that would otherwise appear equal in their propensity for outbreaks (e.g., similar climate conditions). We also show that the model captures the peak timing of outbreaks (Fig. 3b) and outbreak duration (Fig. 3c) but not the final outbreak size (Fig. 3d) or maximum number of infections (Fig. 3e), supporting the hypothesis that the magnitude of disease cases during an outbreak in settings with year-round climate suitability for disease transmission are invariant to temperature, as proposed by [30], likely because the magnitude of disease cases is probably more strongly driven by the availability of susceptible hosts.

Given that the model generally did not predict the magnitude of outbreaks, we asked how well the model reproduced vector and human disease dynamics (i.e., variation over time) across sites and whether this relationship varied systematically with different socio-economic factors. Across sites, the range of temporal correlations between model predictions and observations (N = 8; Fig. 4, Table 2) provides an informative metric for the proportion of true disease dynamics that we might expect to capture in new settings, ranging from 28 – 88%. The correlations varied with demography, housing construction, and climate (Fig. 6). The model may have better explained vector dynamics in locations with a lower proportion of children under five years old for a variety of reasons, including because bottom-heavy demographic pyramids are often associated with lower socioeconomic status and higher mobility throughout the day. In addition to the demographic makeup of sites, housing construction within sites also seems to modify transmission dynamics: vector dynamics were less predictable in sites with more houses with piped water and made of cement (Fig. 6b,d). These results suggest that piped water may prevent additional contact between humans and mosquitoes associated with stored water around the home. In addition, housing materials like cement that lower indoor temperature could artificially decrease climate suitability for mosquitoes, thereby decreasing the probability that mosquitoes will enter and bite people inside their homes. Despite incorporating all known temperature-dependent mosquito traits into the SEI-SEIR model, we still found vector dynamics became less predictable near the empirically derived thermal optima for arboviral transmission (Figs. 6c, 7). This finding may be associated with physiological or behavioral responses of mosquitoes to temperatures near

409 their thermal safety margin [59,60] and/or humans modifying their environment (as
410 described above) in locations optimal for transmission.
411
412 Across the study sites, we found support for three hypothesized relationships between
413 rainfall and mosquito carrying capacity as well as several time lags between model
414 predictions and disease observations. Support for multiple rainfall functions could
415 indicate that the effects of rainfall on immature habitat is highly heterogenous, which has
416 been found in previous research in Ecuador [27] and Kenya [61]. Alternatively, the
417 combination of multiple rainfall relationships and time lags could arise from nonlinear
418 and delayed effects of extreme climate such as droughts and floods. More specifically,
419 we hypothesize that there may be multiple mechanistic relationships for the effects of
420 rainfall on mosquito abundance and arboviral disease dynamics (Fig. 5), and they may act
421 on different time scales. For example, previous research indicated that dengue outbreaks
422 were more likely to occur four to five months after a drought and one month after
423 excessive rainfall and a statistical model that incorporated these duel exposure-lag-
424 response functions was highly effective at predicting dengue outbreaks in Barbados [62].
425 Further, if multiple rainfall relationships act in concert across varying time lags, this
426 would help to explain why many different time lags have been observed between rainfall
427 and arboviral dynamics in previous studies [6,27,51,63–65].
428
429 Future research can build on this study to improve our understanding of arboviral
430 dynamics across settings. There were several factors that we did not include in this study,
431 such as existing vector control programs, infrastructure, and preexisting immunity in the

population. For instance, in Ecuador, factors such as distance to abandoned properties, interruptions in access to piped water, shaded patios, and use of vector control are documented to influence arbovirus transmission [66], whereas in the study sites in Kenya, factors associated with arboviral transmission are less well studied and there are currently no widely used vector control or local arboviral surveillance programs employed. Future studies could further improve the model by incorporating human immune dynamics associated with interactions among different dengue serotypes [67] or cross-reactivity among viral antibodies [68], differential susceptibility across human age classes [69], and heterogeneity in contact rates between mosquitoes and people based on human behavior and movement [70,71]. Further, as experimental data becomes available for trait estimates specific to chikungunya and Zika, this model could be partitioned to model each arboviral disease individually. This is likely to be an important addition as the different arboviruses tend to peak in different years, possibility due to differences in viral development rates and extrinsic incubation periods among arboviruses. Therefore, validating the model with all three arboviruses combined may oversimplify the complex interannual dynamics that arise due to competition among arboviruses in mosquitoes and humans. There were not enough data for chikungunya and Zika cases in this study to formally test such patterns. This study provides strong evidence that a trait-based model, parameterized independently from field data, can reproduce key epidemic characteristics and a range of spatiotemporal arboviral disease dynamics. Such mechanistic, climate-driven models will become increasingly important to support public health efforts in the face of novel climate regimes emerging due to climate change.

Materials and Methods:

Climate data

We collected *in situ* measurements of daily mean temperature, relative humidity, and rainfall at each study site and interpolated missing data where necessary. We used temperature and humidity measurements from HOBO loggers and rainfall measurements from rain gauges for sites in Kenya. We used temperature, humidity, and rainfall measurements from automatic weather stations operated by the National Institute of Meteorology and Hydrology in Ecuador. For Kenya, we interpolated missing temperature data from NOAA Global Surface Summary of the Day (Table S2, Fig. S4) and interpolated missing rainfall data from NOAA Climate Prediction Center Africa Rainfall Climatology dataset (Table S2, Fig. S5). For Ecuador, we interpolated missing temperature (Table S2, Fig. S4) and rainfall (Table S2, Fig. S5) data using the nearest study site where possible and otherwise based on long term mean values for the corresponding Julian day. To interpolate missing data, we linearly regressed all measurements taken on the same day in two datasets and then used the linear model to interpolate temperature for the site with missing data based on the climate measurement from the secondary source for the date when the data was missing (Figs. S4-5). For rainfall, we first calculated a moving window of 14-day accumulated rainfall (which is short enough to capture variability and seasonality in rainfall patterns and follows [72]) for each day before interpolation because modeled daily rainfall values are less reliable than accumulated rainfall over a two week period. We interpolated 14-day cumulative rainfall for any day with a missing rainfall value in the prior 14 days. For both Kenya and Ecuador, we interpolated missing relative humidity data based on long term mean values

for the corresponding Julian day (Table S2). We then calculated the saturation vapor pressure deficit (SVPD) from temperature and humidity to use in the humidity function because previous research suggests SVPD is a more informative measure of the effect of humidity on mosquito survival compared with relative humidity [73]. To calculate SVPD, we first calculated the saturation vapor pressure as:

$$SVP = 610.7 * 10^{7.5*T/(273.3+T)} \quad (1)$$

where (T) is temperature in degrees Celsius. We then calculated SVPD (in kilopascals) as

$$SVPD = 1 - \frac{RH}{100} * SVP \quad (2)$$

where RH is relative humidity. The final dataset had no missing values for temperature (Fig. S6), rainfall (Fig. S7), and humidity (Fig. S8).

Vector surveys

We collected, counted, sexed, and classified mosquitoes by species, and aggregated the data to mean number of *Aedes aegypti* per house, month, year, and site to account for differences in survey effort across months and sites. We collected adult mosquitoes using Prokopack aspirators [74]. In Ecuador, we collected mosquitoes from approximately 27 houses per site (range = 3-57 houses across four sites) every one-to-two weeks during three, four-month sampling periods between July 2016 and August 2018 (≈ 37 sampling weeks per site) to capture different parts of the transmission season. We aggregated the Ecuador vector data to monthly values (≈ 15 sampling months per site) to correspond with the temporal resolution of surveys in Kenya. In Kenya, we collected mosquitoes from approximately 20 houses per site (range = 1-47 houses across four sites) every month between January 2014 and October 2018 (≈ 54 sampling months per site). In

Kenya, we also collected pupae, late instars, and early instars from containers with standing water around the home and collected eggs by setting ovitraps for an average of four days in and around each house monthly. We brought pupae, late and early instars, and eggs to the insectary and reared them to adulthood to classify individuals by sex and species. All mosquito traps capture a small portion of the true mosquito population; therefore, using consistent trapping methods at the same locations through time allows us to compare relative mosquito population dynamics across study sites rather than the absolute magnitude of mosquito abundances.

Arboviral surveys

For Ecuador, we analyzed laboratory-confirmed dengue, chikungunya, and Zika cases provided by the Ministry of Health (MoH) of Ecuador. The MoH collects serum samples from a subset of people with suspected arbovirus infections, and samples are tested at the National Public Health Research Institute by molecular diagnostics (RT-PCR) or antibody tests (IgM ELISA for dengue), depending on the number of days of illness. Results are sent to the MoH Epidemiological Surveillance and Control National Directorate (SIVE Alerta system). Laboratory-confirmed dengue cases were available for all four sites from 2014 to 2018. Laboratory-confirmed chikungunya cases were available for Machala and Huaquillas from 2015 to 2018. Laboratory-confirmed Zika cases were available for Machala from 2016 to 2018.

For Kenya, we used laboratory-confirmed dengue cases aggregated by site and month between 2014 and 2018 collected in a passive surveillance study on childhood febrile

illness in Kenya (NIH R01AI102918, PI: ADL). The study population consisted of 7,653 children less than 18 years of age with undifferentiated febrile illness. Children with fever enrolled in the study when attending outpatient care in one of the four study sites (Mbaka Oromo Health Centre in Chulaimbo, Obama Children's Hospital in Kisumu, Msambweni District Hospital in Msambweni, and Ukunda/Diani Health Center in Ukunda). Local health officers collected comprehensive clinical and demographic data and phlebotomy at the initial visit. We tested each child's blood for dengue viremia by molecular diagnostics (conventional PCR [75] or targeted multiplexed real-time PCR when available [76]), or serologic conversion between an initial and a follow up visit (IgG ELISA [77]).

For arboviral data collection in Ecuador and Kenya, participants provided consent and all local and institutional protocols were followed.

SEI-SEIR model

We adapted an SEI-SEIR model parameterized for dengue transmission in *Ae. aegypti* mosquitoes [30] to simulate mosquito abundance and arboviral cases through time based on daily weather conditions in eight study locations. The model (equations 3-9; Fig. 2), created independently from the observed data described above, allows mosquito life history traits and viral development rate to vary with temperature (T) following [30], mosquito carrying capacity to vary with accumulated 14-day rainfall (R) following [72], and mosquito mortality to vary with humidity (i.e., saturation vapor pressure deficit) (H) following [73].

$$\frac{dS_m}{dt} = \varphi(T,H) * \frac{1}{\mu(T,H)} * N_m * \left(1 - \frac{N_m}{K(T,R,H)}\right) - \left(a(T) * pMI(T) * \frac{I_h}{N_h} + \mu(T,H)\right) * S_m \quad (3)$$

$$\frac{dE_m}{dt} = a(T) * pMI(T) * \frac{I_h}{N_h} * S_m - \left(PDR(T) + \mu(T,H)\right) * E_m \quad (4)$$

$$\frac{dI_m}{dt} = PDR(T) * E_m - \mu(T,H) * I_m \quad (5)$$

$$\frac{dS_h}{dt} = -a(T) * b(T) * \frac{I_m}{N_h} * S_h + BR * S_h - DR * S_h + ie * N_h - ie * S_h \quad (6)$$

$$\frac{dE_h}{dt} = a(T) * b(T) * \frac{I_m}{N_h} * S_h - \delta * E_h - DR * E_h - ie * E_h \quad (7)$$

$$\frac{dI_h}{dt} = \delta * E_h - \eta * I_h - DR * I_h - ie * I_h \quad (8)$$

$$\frac{dR_h}{dt} = \eta * I_h - DR * R_h - ie * R_h \quad (9)$$

where

$$\varphi(T,H) = EFD(T) * pEA(T) * MDR(T) \quad (10)$$

The adult mosquito population (N_m) is separated into susceptible (S_m), exposed (E_m), and infectious (I_m) compartments and the human population (N_h) is separated into susceptible (S_h), exposed (E_h), infectious (I_h), and recovered (R_h) compartments (Fig. 2). Climate-independent model parameters (Table 3) include the intrinsic incubation period (δ), human infectivity period (η), birth rate (BR), death rate (DR), and immigration/emigration rate (ie). The temperature-dependent SEI-SEIR model was developed by Huber et al. [30] and allows mosquito life history traits and viral development rate to vary according to thermal response curves fit from data derived in laboratory experiments conducted at constant temperatures (Table 3). Although laboratory experiments do not reflect real-world conditions, the physiological responses measured are biologically meaningful. The temperature-dependent traits include eggs laid per female per day (EFD), the probability of egg-to-adult survival (pEA), mosquito development rate (MDR), mosquito mortality rate (lifespan^{-1}; μ), biting rate (a), probability of mosquito infection per bite on an infectious

560 host (pMI), parasite development rate (PDR), and probability of mosquito infectiousness
561 given an infectious bite (b). We modified the mosquito mortality rate equation to vary as
562 a function of temperature and humidity by fitting a spline model based on a pooled
563 survival analysis of *Ae. aegypti* [73] (Fig. S9):

$$\mu(T,H) = \frac{1}{c*(T-T_0)*(T-T_m)} + (1-(0.01+2.01*H))*y \qquad H<1 \qquad (11)$$

$$\mu(T,H) = \frac{1}{c*(T-T_0)*(T-T_m)} + (1-(1.22+0.27*H))*y \qquad H\geq 1 \qquad (12)$$

564 where the rate constant (c), minimum temperature (T_0), and maximum temperature (T_m)
565 equal -1.24, 16.63, and 31.85 respectively (Table 4), humidity (H) is the saturation vapor
566 pressure deficit, and y is a scaling factor that we set to 0.005 and 0.01, respectively, to
567 restrict mosquito mortality rates within the range of mortality rates estimated by other
568 studies [19,73]. The linear humidity function has a steeper slope at lower humidity values
569 (equation 11) compared with higher humidity values (equation 12) based on previous
570 research [73] (Fig. S9).
571
572 We modeled adult mosquito carrying capacity, K, as a modified Arrhenius equation
573 following [30,78]:

$$K(T,H,R) = \frac{EFD(T_0)*pEA(T_0)*MDR(T_0)*\mu(T_0,H_0)^{-1} - \mu(T_0,H_0)}{EFD(T_0)*pEA(T_0)*MDR(T_0)*\mu(T_0,H_0)^{-1}} * N_{m.max} \qquad (13)$$
$$* e^{\frac{-E_A*(T-T_0)^2}{\kappa_B*(T+273)*(T_0+273)}} * f(R)$$

574 with T_0 and H_0 set to the temperature and humidity where carrying capacity is greatest (i.e.,
575 physiological optimal conditions from laboratory experiments; 29°C and 6 kPA), $N_{m.max}$
576 set to the maximum possible mosquito abundance in a population (twice the human
577 population size following [30]), and the Boltzmann constant, (K_B), is 8.617 x 10^{-5} eV/K.

We set the activation energy, E_A, as 0.05 based on [30]. Since there were no experimental data from which to derive the functional response of mosquito carrying capacity across a gradient of rainfall values, we tested several functional relationships based on hypothesized biological relationships between freshwater availability and immature mosquito breeding habitat, modeling the effect of rainfall on carrying capacity, $f(R)$, as either:

$$f(R_{\text{Brière}}) = c * R * (R - R_{min}) * \sqrt{(R_{max} - R)} * z \quad (14)$$

$$f(R_{Quadratic}) = c * (R - R_{min}) * (R - R_{max}) * z \quad (15)$$

$$f(R_{\text{Inverse}}) = \frac{1}{R} * z \quad (16)$$

where minimum rainfall (R_{min}) equaled 1 mm and maximum rainfall (R_{max}) equaled 123 mm based on the high probability of flushing [26]. The quadratic function is similar to the rainfall function found in [26] and the inverse function is based on the rainfall function used in [72]. We used rate constants (c) of $7.86e^{-5}$ and $-5.99e^{-3}$ for the Brière and quadratic functions respectively, based on rate constants for other parameters with similar functional forms (Table 4). We also included a scaling factor, z (0. 28, 0.025, and 0.60 respectively), to restrict the maximum carrying capacity to produce model outputs based on a subsample of the total population for comparison with observations. Since the rate constant, c, is multiplied by z, inferring the exact value of c is not necessary because it is scaled by z. The scaling factor could be removed from the model to simulate dynamics in the total population.

598 **Table 3: Values of temperature-invariant parameters used in the model.** We derived
599 daily birth and death rates in the model by dividing the per capita birth and death rates by
600 360 days. The World Bank Open Data can be found at https://data.worldbank.org/.

Parameter	Definition	Value	Source
δ^{-1}	Intrinsic incubation period (days)	5.9	[30]
η^{-1}	Human infectivity period (days)	5.0	[30]
BR	Annual birth rate (per 1000 people)	31.782 (Ecuador) 20.175 (Kenya)	The World Bank Open Data
DR	Annual death rate (per 1000 people)	5.284 (Ecuador) 5.121 (Kenya)	The World Bank Open Data
ie	Immigration/emigration rate	0.01	Expert opinion

601
602
603
604
605
606
607
608
609
610
611
612
613

Table 4: Fitted thermal responses for *Ae. aegypti* life history traits. Traits were fit to a Brière $[cT(T-T_0)(T_m-T)^{\frac{1}{2}}]$ or a quadratic $[c(T-T_m)(T-T_0)]$ function where T represents temperature. T_0 and T_m are the critical thermal minimum and maximum, respectively, and c is the rate constant. Thermal responses were fit by [19] and also used in [30]. Parasite development rate was measured as the virus extrinsic incubation rate.

Trait	Definition	Function	c	T_0	T_m
a	Biting rate (day^{-1})	Brière	2.71×10^{-04}	14.67	41.00
EFD	Eggs laid per female per day	Brière	2.08×10^{-02}	14.06	32.03
pEA	Probability of mosquito egg-to-adult survival	Quadratic	-3.36×10^{-03}	7.68	38.31
MDR	Mosquito egg-to-adult development rate (day^{-1})	Brière	1.49×10^{-04}	15.12	37.67
Lf	Adult mosquito lifespan (days)	Quadratic	-1.24	16.63	31.85
b	Probability of mosquito infectiousness	Brière	9.86×10^{-04}	12.05	32.79
pMI	Probability of mosquito infection	Brière	5.23×10^{-04}	1.51	34.74
PDR	Parasite development rate (day^{-1})	Brière	1.04×10^{-04}	11.50	38.97

To initiate the model, we used site-specific values for human population size and randomly selected one set of values for all sites for the proportion of mosquitoes and humans in each compartment. For Ecuador, we used population estimates from official population projections produced by Proyección de la Población Ecuatoriana, por años calendario, según cantones 2010-2020 (https://www.ecuadorencifras.gob.ec/proyecciones-poblacionales/) with population sizes of 57,366, 279,887, 13,673, and 25,615 for Huaquillas, Machala, Portovelo, and Zaruma, respectively, based on 2017 projections. For Kenya, we estimated the population sizes

628 served by each outpatient care facility by creating a polygon around all the geolocations
629 of study participants' homes enrolled at each outpatient care facility and summed
630 population count data from NASA's Socioeconomic Data and Applications Center
631 Gridded Population of the World v4 (https://doi.org/10.7927/H4JW8BX5) within each
632 polygon using ArcGIS v 10.4.1. We estimated population sizes of 7,304, 547,557,
633 240,698, and 154,048 for Chulaimbo, Kisumu, Msambweni, and Ukunda, respectively.
634 We set the ratio of mosquitoes to humans to two, following [30]. We used the following
635 values as the initial proportion of mosquitoes and humans in each model compartment:
636 S_m = 0.22, E_m = 0.29, I_m = 0.49, S_h = 0.58, E_h = 0.22, I_h = 0.00, and R_h = 0.20. We
637 determined that the model was invariant to initial proportion values after a short burn-in
638 period (90 days) based on a sensitivity analysis (Fig. S10); therefore, we randomly
639 selected one set of initial proportion values from the sensitivity analysis for all the model
640 simulations. We also determined that the temporal trajectories of model dynamics did not
641 change when we varied the critical thermal minimum, maximum, and rate constants
642 (Table 4) for *Aedes aegypti* life history traits (Fig. S1-2).
643
644 We ran all model simulations using the deSolve package in R statistical software v 3.5.3
645 [79].
646
647 Model validation
648 To validate the SEI-SEIR model, we calculated pairwise correlations with an adjusted p-
649 value to account for autocorrelation for each site. For the pairwise correlations, we used
650 the ccf function in base R [79] to calculate correlations between the two times series of

model predictions and observations with 0, 1, 2, 3, 4, and 5-month lags. We then calculated an adjusted p-value using the Modified Chelton method [45] to adjust the null hypothesis test of sample correlation between autocorrelated time series. To assess predictions and observations for vector dynamics for each site, we compared monthly time series of the total predicted mosquito population from the SEI-SEIR model with the monthly time series of mean number of *Aedes aegypti* (per house). We followed the same procedure to compare model predictions with other mosquito life stages for sites in Kenya. Similarly, to compare predictions and observations for human disease dynamics for each site, we compared monthly times series of predicted infected individuals from the SEI-SEIR model with the monthly time series of total laboratory-confirmed arboviral cases. For subsequent analyses, we used model predictions from the model (e.g., SEI-SEIR model with a specific rainfall function and time lag) with the highest pairwise correlation value.

To compare key epidemic characteristics between model predictions and observations and to compare site-specific correlations with socio-economic factors, we used linear regression models using the lm function in that stats package in R [79]. We defined outbreaks as a continuous time period where the peak cases exceeded the mean number of cases (predicted or observed) plus one standard deviation within a site. We then used those outbreak periods to count the total number of outbreaks within each site, and, for predicted and observed outbreaks that overlapped in time, the duration, peak timing total outbreak size, and maximum number of infections. We compared predictions and observations for each of these metrics with linear regression. Since we were interested in

674 whether model predictions matched observations for each independent outbreak period,
675 we did not allow varying intercepts or slopes by site. Similarly, we compared the
676 pairwise correlation values (described above) across all sites with each socio-economic
677 factor listed in Table 1 separately using linear regressions.
678
679 Comparison of R_0 with prior studies
680 We collected effect sizes of temperature on dengue incidence from 12 peer-reviewed
681 studies from the literature (Table S1). We selected studies with mean temperatures across
682 the predicted temperature range where arboviral transmission can occur. We scaled the
683 coefficient values to visualize the relative effect of temperature across studies given that
684 the original analyses were conducted with different temperature metrics and across
685 different temperature ranges. We provide additional information and sources in Table S1.
686
687 **Data availability statement:** Climate data, epidemic characteristics data, and socio-
688 economic data are available at https://github.com/jms5151/SEI-SEIR_Arboviruses. We
689 used this data to create figures 3, 4, and 6 in the main text and supplemental figures 1-3
690 and 6-10; we provide the data used in figure 7 in supplemental table 1. We can provide
691 vector and arboviral case data upon request with permission from appropriate data
692 providers (e.g., Ecuador Ministry of Health).
693
694 **Code availability:** Model and analysis codes are available at
695 https://github.com/jms5151/SEI-SEIR_Arboviruses.
696

Acknowledgements: JMC, ADL, EFL, and EAM were supported by a Stanford Woods Institute for the Environment – Environmental Ventures Program grant (PIs: EAM, ADL, and EFL). EAM was also supported by a Hellman Faculty Fellowship and a Terman Award. ADL, BAN, FMM, ENGS, MSS, ARK, RD, AA, and HNN were supported by a National Institutes of Health R01 grant (AI102918; PI: ADL). EAM, AMSI, and SJR were supported by a National Science Foundation (NSF) Ecology and Evolution of Infectious Diseases (EEID) grant (DEB-1518681) and AMSI and SJR were also supported by an NSF DEB RAPID grant (1641145). EAM was also supported by a National Institute of General Medical Sciences Maximizing Investigators' Research Award grant (R35GM133439) and an NSF and Fogarty International Center EEID grant (DEB-2011147). We thank Cat Lippi for assistance with formatting household quality survey data from Ecuador.

Author contributions: EAM, ADL, EFL, and JMC conceived of project. JMC conducted analyses and wrote manuscript. EAM, ADL, EFL, and AMSI secured funding for the project. BNN, FMM, EBA, AA, MJBC, RD, FHH, RM, and HNN collected data. ENGS and MMS conducted laboratory analyses. ARK, SJR, and RS processed data. All authors revised and approved of the manuscript.

720 **References:**

721 1. Ockendon N, Baker DJ, Carr JA, White EC, Almond REA, Amano T, et al.
722 Mechanisms underpinning climatic impacts on natural populations: altered species
723 interactions are more important than direct effects. Glob Chang Biol. 2014;20:
724 2221–2229. doi:10.1111/gcb.12559
725 2. Boggs CL, Inouye DW. A single climate driver has direct and indirect effects on
726 insect population dynamics. Ecol Lett. 2012;15: 502–508. doi:10.1111/j.1461-
727 0248.2012.01766.x
728 3. Burkett VR, Wilcox DA, Stottlemyer R, Barrow W, Fagre D, Baron J, et al.
729 Nonlinear dynamics in ecosystem response to climatic change: Case studies and
730 policy implications. Ecol Complex. 2005;2: 357–394.
731 doi:10.1016/j.ecocom.2005.04.010
732 4. Molnár PK, Sckrabulis JP, Altman KA, Raffel TR. Thermal Performance Curves
733 and the Metabolic Theory of Ecology—A Practical Guide to Models and
734 Experiments for Parasitologists. J Parasitol. 2017;103. doi:10.1645/16-148
735 5. Hortion J, Mutuku FM, Eyherabide AL, Vu DM, Boothroyd DB, Grossi-Soyster
736 EN, et al. Acute Flavivirus and Alphavirus Infections among Children in Two
737 Different Areas of Kenya, 2015. Am J Trop Med Hyg. 2019;100: 170–173.
738 doi:10.4269/ajtmh.18-0297
739 6. Stewart-Ibarra AM, Lowe R. Climate and Non-Climate Drivers of Dengue
740 Epidemics in Southern Coastal Ecuador. Am J Trop Med Hyg. 2013;88: 971–981.
741 doi:10.4269/ajtmh.12-0478
742 7. Jury MR. Climate influence on dengue epidemics in Puerto Rico. Int J Environ

Health Res. 2008;18: 323–334. doi:10.1080/09603120701849836

8. Campbell KM, Haldeman K, Lehnig C, Munayco C V., Halsey ES, Laguna-Torres VA, et al. Weather Regulates Location, Timing, and Intensity of Dengue Virus Transmission between Humans and Mosquitoes. Michael E, editor. PLoS Negl Trop Dis. 2015;9: e0003957. doi:10.1371/journal.pntd.0003957

9. Adde A, Roucou P, Mangeas M, Ardillon V, Desenclos J-C, Rousset D, et al. Predicting Dengue Fever Outbreaks in French Guiana Using Climate Indicators. Scarpino S V., editor. PLoS Negl Trop Dis. 2016;10: e0004681. doi:10.1371/journal.pntd.0004681

10. Dhimal M, Gautam I, Joshi HD, O'Hara RB, Ahrens B, Kuch U, et al. Risk Factors for the Presence of Chikungunya and Dengue Vectors (Aedes aegypti and Aedes albopictus), Their Altitudinal Distribution and Climatic Determinants of Their Abundance in Central Nepal. Turell MJ, editor. PLoS Negl Trop Dis. 2015;9: e0003545. doi:10.1371/journal.pntd.0003545

11. Descloux E, Mangeas M, Menkes CE, Lengaigne M, Leroy A, Tehei T, et al. Climate-Based Models for Understanding and Forecasting Dengue Epidemics. Anyamba A, editor. PLoS Negl Trop Dis. 2012;6: e1470. doi:10.1371/journal.pntd.0001470

12. Aswi A, Cramb SM, Moraga P, Mengersen K. Epidemiology and Infection Bayesian spatial and spatio-temporal approaches to modelling dengue fever: a systematic review. Epidemiol Infect. 2018;147. doi:10.1017/S0950268818002807

13. Johansson MA, Apfeldorf KM, Dobson S, Devita J, Buczak AL, Baugher B, et al. An open challenge to advance probabilistic forecasting for dengue epidemics. Proc

766 Natl Acad Sci. 2019; 201909865. doi:10.1073/pnas.1909865116

767 14. Michael E, Singh BK, Mayala BK, Smith ME, Hampton S, Nabrzyski J.
768 Continental-scale, data-driven predictive assessment of eliminating the vector-
769 borne disease, lymphatic filariasis, in sub-Saharan Africa by 2020. BMC Med.
770 2017;15: 176. doi:10.1186/s12916-017-0933-2

771 15. Smith T, Maire N, Ross A, Penny M, Chitnis N, Schapira A, et al. Towards a
772 comprehensive simulation model of malaria epidemiology and control.
773 Parasitology. 2008. pp. 1507–1516. doi:10.1017/S0031182008000371

774 16. Ryan SJ, Carlson CJ, Mordecai EA, Johnson LR. Global expansion and
775 redistribution of Aedes-borne virus transmission risk with climate change. Han
776 BA, editor. PLoS Negl Trop Dis. 2019;13: e0007213.
777 doi:10.1371/journal.pntd.0007213

778 17. Kraemer MU, Sinka ME, Duda KA, Mylne AQ, Shearer FM, Barker CM, et al.
779 The global distribution of the arbovirus vectors *Aedes aegypti* and *Ae. albopictus*.
780 Elife. 2015;4. doi:10.7554/eLife.08347

781 18. Powell JR, Tabachnick WJ, Powell JR, Tabachnick WJ. History of domestication
782 and spread of Aedes aegypti - A Review. Mem Inst Oswaldo Cruz. 2013;108: 11–
783 17. doi:10.1590/0074-0276130395

784 19. Mordecai EA, Cohen JM, Evans M V., Gudapati P, Johnson LR, Lippi CA, et al.
785 Detecting the impact of temperature on transmission of Zika, dengue, and
786 chikungunya using mechanistic models. Althouse B, editor. PLoS Negl Trop Dis.
787 2017;11: e0005568. doi:10.1371/journal.pntd.0005568

788 20. Shocket MS, Ryan SJ, Mordecai EA. Temperature explains broad patterns of Ross

789 River virus transmission. Elife. 2018; doi:10.7554/eLife.37762.001

790 21. Paull SH, Horton DE, Ashfaq M, Rastogi D, Kramer LD, Diffenbaugh NS, et al.
791 Drought and immunity determine the intensity of West Nile virus epidemics and
792 climate change impacts. Proc R Soc B Biol Sci. 2017;284: 20162078.
793 doi:10.1098/rspb.2016.2078

794 22. Costa EAP de A, Santos EM de M, Correia JC, Albuquerque CMR de. Impact of
795 small variations in temperature and humidity on the reproductive activity and
796 survival of Aedes aegypti (Diptera, Culicidae). Rev Bras Entomol. 2010;54: 488–
797 493. doi:10.1590/S0085-56262010000300021

798 23. Gaaboub IA, El-Sawaf SK, El-Latif MA. Effect of Different Relative Humidities
799 and Temperatures on Egg-Production and Longevity of Adults of Anopheles
800 (Myzomyia) pharoensis Theob.1. Zeitschrift für Angew Entomol. 2009;67: 88–94.
801 doi:10.1111/j.1439-0418.1971.tb02098.x

802 24. Koenraadt CJM, Harrington LC. Flushing Effect of Rain on Container-Inhabiting
803 Mosquitoes Aedes aegypti and Culex pipiens (Diptera: Culicidae). J Med Entomol.
804 2009;45: 28–35. doi:10.1603/0022-2585(2008)45[28:FEOROC]2.0.CO;2

805 25. Paaijmans KP, Wandago MO, Githeko AK, Takken W, Vulule J. Unexpected High
806 Losses of Anopheles gambiae Larvae Due to Rainfall. Carter D, editor. PLoS One.
807 2007;2: e1146. doi:10.1371/journal.pone.0001146

808 26. Benedum CM, Seidahmed OME, Eltahir EAB, Markuzon N. Statistical modeling
809 of the effect of rainfall flushing on dengue transmission in Singapore. Reiner RC,
810 editor. PLoS Negl Trop Dis. 2018;12: e0006935.
811 doi:10.1371/journal.pntd.0006935

812 27. Stewart Ibarra AM, Ryan SJ, Beltrán E, Mejía R, Silva M, Muñoz Á. Dengue
813 Vector Dynamics (Aedes aegypti) Influenced by Climate and Social Factors in
814 Ecuador: Implications for Targeted Control. Mores CN, editor. PLoS One. 2013;8:
815 e78263. doi:10.1371/journal.pone.0078263
816 28. Pontes RJ, Spielman A, Oliveira-Lima JW, Hodgson JC, Freeman J. Vector
817 densities that potentiate dengue outbreaks in a Brazilian city. Am J Trop Med Hyg.
818 2000;62: 378–383. doi:10.4269/ajtmh.2000.62.378
819 29. Anyamba A, Linthicum KJ, Small JL, Collins KM, Tucker CJ, Pak EW, et al.
820 Climate Teleconnections and Recent Patterns of Human and Animal Disease
821 Outbreaks. Zhou X-N, editor. PLoS Negl Trop Dis. 2012;6: e1465.
822 doi:10.1371/journal.pntd.0001465
823 30. Huber JH, Childs ML, Caldwell JM, Mordecai EA. Seasonal temperature variation
824 influences climate suitability for dengue, chikungunya, and Zika transmission.
825 Althouse B, editor. PLoS Negl Trop Dis. 2018;12: e0006451.
826 doi:10.1371/journal.pntd.0006451
827 31. Lourenço J, Recker M. The 2012 Madeira Dengue Outbreak: Epidemiological
828 Determinants and Future Epidemic Potential. Scarpino S V., editor. PLoS Negl
829 Trop Dis. 2014;8: e3083. doi:10.1371/journal.pntd.0003083
830 32. Li R, Xu L, Bjørnstad ON, Liu K, Song T, Chen A, et al. Climate-driven variation
831 in mosquito density predicts the spatiotemporal dynamics of dengue. Proc Natl
832 Acad Sci. 2019;119: 3624–3629. doi:10.1073/PNAS.1806094116
833 33. Wang X, Tang S, Cheke RA. A stage structured mosquito model incorporating
834 effects of precipitation and daily temperature fluctuations. J Theor Biol. 2016;411:

27–36. doi:10.1016/j.jtbi.2016.09.015

34. Siraj AS, Oidtman RJ, Huber JH, Kraemer MUG, Brady OJ, Johansson MA, et al. Temperature modulates dengue virus epidemic growth rates through its effects on reproduction numbers and generation intervals. Althouse B, editor. PLoS Negl Trop Dis. 2017;11: e0005797. doi:10.1371/journal.pntd.0005797

35. Oidtman RJ, Lai S, Huang Z, Yang J, Siraj AS, Reiner RC, et al. Inter-annual variation in seasonal dengue epidemics driven by multiple interacting factors in Guangzhou, China. Nat Commun. 2019;10. doi:10.1038/s41467-019-09035-x

36. Stewart-Ibarra AM, Muñoz ÁG, Ryan SJ, Ayala EB, Borbor-Cordova MJ, Finkelstein JL, et al. Spatiotemporal clustering, climate periodicity, and social-ecological risk factors for dengue during an outbreak in Machala, Ecuador, in 2010. BMC Infect Dis. 2014;14: 610. doi:10.1186/s12879-014-0610-4

37. Agha SB, Tchouassi DP, Turell MJ, Bastos ADS, Sang R. Entomological assessment of dengue virus transmission risk in three urban areas of Kenya. Reiner RC, editor. PLoS Negl Trop Dis. 2019;13: e0007686. doi:10.1371/journal.pntd.0007686

38. Agha SB, Tchouassi DP, Bastos ADS, Sang R. Dengue and yellow fever virus vectors: seasonal abundance, diversity and resting preferences in three Kenyan cities. Parasit Vectors. 2017;10: 628. doi:10.1186/s13071-017-2598-2

39. Chretien J-P, Anyamba A, Bedno SA, Breiman RF, Sang R, Sergon K, et al. Drought-Associated Chikungunya Emergence Along Coastal East Africa. Am J Trop Med Hyg. 2007;76: 405–407. doi:10.4269/ajtmh.2007.76.405

40. Vu DM, Mutai N, Heath CJ, Vulule JM, Mutuku FM, Ndenga BA, et al.

Unrecognized Dengue Virus Infections in Children, Western Kenya, 2014-2015. Emerg Infect Dis. 2017;23: 1915–1917. doi:10.3201/eid2311.170807

41. Gubler DJ, Nalim S, Saroso JS, Saipan H, Tan R. Variation in Susceptibility to Oral Infection with Dengue Viruses among Geographic Strains of Aedes Aegypti *. Am J Trop Med Hyg. 1979;28: 1045–1052. doi:10.4269/ajtmh.1979.28.1045

42. Xavier-Carvalho C, Chester Cardoso C, de Souza Kehdya F, Guilherme Pacheco A, Ozório Moraesa M. Host genetics and dengue fever. Infect Genet Evol. 2017;56: 99–110. doi:10.1016/J.MEEGID.2017.11.009

43. Didan K, Barreto Munoz A, Solano R, Huete A. MODIS Vegetation Index User's Guide (MOD13 Series) [Internet]. Available: http://vip.arizona.edu

44. Sulla-Menashe D, Friedl MA. User Guide to Collection 6 MODIS Land Cover (MCD12Q1 and MCD12C1) Product. 2018; doi:10.5067/MODIS/MCD12Q1

45. Pyper BJ, Peterman RM. Comparison of methods to account for autocorrelation in correlation analyses of fish data. Can J Fish Aquat Sci. 1998;55: 2127–2140. doi:10.1139/f98-104

46. Shocket MS, Anderson CB, Caldwell JM, Childs ML, Han S, Harris M, et al. Environmental drivers of vector-borne disease. Population Biology of Vector-borne Diseases. Oxford University Press;

47. Hurtado-Daz M, Riojas-Rodrguez H, Rothenberg S, Gomez-Dantes H, Cifuentes E. Impact of climate variability on the incidence of dengue in Mexico. Trop Med Int Heal. 2007;12. doi:10.1111/j.1365-3156.2007.01930.x

48. Colón-González FJ, Bentham G, Lake IR. Climate Variability and Dengue Fever in Warm and Humid Mexico. Am J Trop Med Hyg. 2011;84: 757–763.

881 doi:10.4269/ajtmh.2011.10-0609

882 49. Wang C, Jiang B, Fan J, Wang F, Liu Q. A Study of the Dengue Epidemic and
883 Meteorological Factors in Guangzhou, China, by Using a Zero-Inflated Poisson
884 Regression Model. Asia Pacific J Public Heal. 2014;26: 48–57.
885 doi:10.1177/1010539513490195

886 50. Minh An DT, Rocklöv J. Epidemiology of dengue fever in Hanoi from 2002 to
887 2010 and its meteorological determinants. Glob Health Action. 2014;7: 23074.
888 doi:10.3402/gha.v7.23074

889 51. Laureano-Rosario AE, Garcia-Rejon JE, Gomez-Carro S, Farfan-Ale JA, Muller-
890 Kargera FE. Modelling dengue fever risk in the State of Yucatan, Mexico using
891 regional-scale satellite-derived sea surface temperature. Acta Trop. 2017;172: 50–
892 57. doi:10.1016/j.actatropica.2017.04.017

893 52. Wu P-C, Guoa H-R, Lung S-C, Lin C-Y, Su H-J. Weather as an effective predictor
894 for occurrence of dengue fever in Taiwan. Acta Trop. 2007;103: 50–57.
895 doi:10.1016/j.actatropica.2007.05.014

896 53. Karim MN, Munshi SU, Anwar N, Alam MS. Climatic factors influencing dengue
897 cases in Dhaka city: a model for dengue prediction. Indian J Med Res. 2012;136:
898 32–9. Available: http://www.ncbi.nlm.nih.gov/pubmed/22885261

899 54. Nakhapakorn K, Tripathi N. An information value based analysis of physical and
900 climatic factors affecting dengue fever and dengue haemorrhagic fever incidence.
901 Int J Health Geogr. 2005;4: 13. doi:10.1186/1476-072X-4-13

902 55. Gharbi M, Quenel P, Gustave J, Cassadou S, Ruche G La, Girdary L, et al. Time
903 series analysis of dengue incidence in Guadeloupe, French West Indies:

Forecasting models using climate variables as predictors. BMC Infect Dis. 2011;11: 166. doi:10.1186/1471-2334-11-166

56. Sharmin S, Glass K, Viennet E, Harley D. Interaction of Mean Temperature and Daily Fluctuation Influences Dengue Incidence in Dhaka, Bangladesh. Kasper M, editor. PLoS Negl Trop Dis. 2015;9: e0003901. doi:10.1371/journal.pntd.0003901

57. Sriprom M, Chalvet-Monfray K, Chaimane T, Vongsawat K, Bicout DJ. Monthly district level risk of dengue occurrences in Sakon Nakhon Province, Thailand. Sci Total Environ. 2010;408: 5521–5528. doi:10.1016/J.SCITOTENV.2010.08.024

58. Martínez-Bello D, López-Quílez A, Prieto AT. Spatiotemporal modeling of relative risk of dengue disease in Colombia. Stoch Environ Res Risk Assess. 2018;32: 1587–1601. doi:10.1007/s00477-017-1461-5

59. Mordecai EA, Caldwell JM, Grossman MK, Lippi CA, Johnson LR, Neira M, et al. Thermal biology of mosquito-borne disease. Byers J (Jeb), editor. Ecol Lett. 2019; ele.13335. doi:10.1111/ele.13335

60. Carrington LB, Armijos MV, Lambrechts L, Barker CM, Scott TW. Effects of Fluctuating Daily Temperatures at Critical Thermal Extremes on Aedes aegypti Life-History Traits. PLoS One. 2013;8. doi:10.1371/journal.pone.0058824

61. Ngugi HN, Mutuku FM, Ndenga BA, Musunzaji PS, Mbakaya JO, Aswani P, et al. Characterization and productivity profiles of Aedes aegypti (L.) breeding habitats across rural and urban landscapes in western and coastal Kenya. Parasit Vectors. 2017;10: 331. doi:10.1186/s13071-017-2271-9

62. Lowe R, Gasparrini A, Van Meerbeeck CJ, Lippi CA, Mahon R, Trotman AR, et al. Nonlinear and delayed impacts of climate on dengue risk in Barbados: A

927 modelling study. PLoS Med. 2018;15. doi:10.1371/journal.pmed.1002613

928 63. Li C, Wang X, Wu X, Liu J, Ji D, Du J. Modeling and projection of dengue fever
929 cases in Guangzhou based on variation of weather factors. Sci Total Environ.
930 2017;605–606: 867–873. doi:10.1016/j.scitotenv.2017.06.181

931 64. Li CF, Lim TW, Han LL, Fang R. Rainfall, abundance of Aedes aegypti and
932 dengue infection in Selangor, Malaysia. Southeast Asian J Trop Med Public
933 Health. 1985;16: 560–8. Available: http://www.ncbi.nlm.nih.gov/pubmed/3835698

934 65. Johansson MA, Dominici F, Glass GE. Local and Global Effects of Climate on
935 Dengue Transmission in Puerto Rico. Massad E, editor. PLoS Negl Trop Dis.
936 2009;3: e382. doi:10.1371/journal.pntd.0000382

937 66. Kenneson A, Beltrán-Ayala E, Borbor-Cordova MJ, Polhemus ME, Ryan SJ, Endy
938 TP, et al. Social-ecological factors and preventive actions decrease the risk of
939 dengue infection at the household-level: Results from a prospective dengue
940 surveillance study in Machala, Ecuador. Messer WB, editor. PLoS Negl Trop Dis.
941 2017;11: e0006150. doi:10.1371/journal.pntd.0006150

942 67. Reich NG, Shrestha S, King AA, Rohani P, Lessler J, Kalayanarooj S, et al.
943 Interactions between serotypes of dengue highlight epidemiological impact of
944 cross-immunity. J R Soc Interface. 2013;10: 20130414.
945 doi:10.1098/rsif.2013.0414

946 68. Wen J, Elong Ngono A, Regla-Nava JA, Kim K, Gorman MJ, Diamond MS, et al.
947 Dengue virus-reactive CD8+ T cells mediate cross-protection against subsequent
948 Zika virus challenge. Nat Commun. 2017;8: 1459. doi:10.1038/s41467-017-
949 01669-z

950 69. Rodriguez-Barraquer I, Salje H, Cummings DA. Opportunities for improved
951 surveillance and control of dengue from age-specific case data. Elife. 2019;8.
952 doi:10.7554/eLife.45474
953 70. Stoddard ST, Forshey BM, Morrison AC, Paz-Soldan VA, Vazquez-Prokopec
954 GM, Astete H, et al. House-to-house human movement drives dengue virus
955 transmission. Proc Natl Acad Sci U S A. 2013;110: 994–999.
956 doi:10.1073/pnas.1213349110
957 71. Wesolowski A, Qureshi T, Boni MF, Sundsøy PR, Johansson MA, Rasheed SB, et
958 al. Impact of human mobility on the emergence of dengue epidemics in Pakistan.
959 Proc Natl Acad Sci. 2015;112: 11887–11892. doi:10.1073/pnas.1504964112
960 72. Vaidya A, Bravo-Salgado AD, Mikler AR. Modeling climate-dependent
961 population dynamics of mosquitoes to guide public health policies. Proc 5th ACM
962 Conf Bioinformatics, Comput Biol Heal Informatics - BCB '14. 2014; 380–389.
963 doi:10.1145/2649387.2649415
964 73. Schmidt CA, Comeau G, Monaghan AJ, Williamson DJ, Ernst KC. Effects of
965 desiccation stress on adult female longevity in Aedes aegypti and Ae. albopictus
966 (Diptera: Culicidae): results of a systematic review and pooled survival analysis.
967 Parasit Vectors. 2018;11: 267. doi:10.1186/s13071-018-2808-6
968 74. Vazquez-Prokopec GM, Galvin WA, Kelly R, Kitron U. A New, Cost-Effective,
969 Battery-Powered Aspirator for Adult Mosquito Collections. J Med Entomol.
970 2009;46: 1256–1259. doi:10.1603/033.046.0602
971 75. Waggoner JJ, Gresh L, Mohamed-Hadley A, Ballesteros G, Davila MJV, Tellez Y,
972 et al. Single-Reaction Multiplex Reverse Transcription PCR for Detection of Zika,

973 Chikungunya, and Dengue Viruses. Emerg Infect Dis. 2016;22: 1295–7.
974 doi:10.3201/eid2207.160326
975 76. Lanciotti RS, Calisher CH, Gubler DJ, Chang GJ, Vorndam A V. Rapid detection
976 and typing of dengue viruses from clinical samples by using reverse transcriptase-
977 polymerase chain reaction. J Clin Microbiol. 1992;30: 545–51. Available:
978 http://www.ncbi.nlm.nih.gov/pubmed/1372617
979 77. Grossi-Soyster EN, Cook EAJ, de Glanville WA, Thomas LF, Krystosik AR, Lee
980 J, et al. Serological and spatial analysis of alphavirus and flavivirus prevalence and
981 risk factors in a rural community in western Kenya. Bingham A, editor. PLoS Negl
982 Trop Dis. 2017;11: e0005998. doi:10.1371/journal.pntd.0005998
983 78. Palamara GM, Childs DZ, Clements CF, Petchey OL, Plebani M, Smith MJ.
984 Inferring the temperature dependence of population parameters: The effects of
985 experimental design and inference algorithm. Ecol Evol. 2014;4: 4736–4750.
986 doi:10.1002/ece3.1309
987 79. Team RC. R: A Language and Environment for Statistical Computing. R Found
988 Stat Comput. 2018; Available: https://www.r-project.org
989